Concentration dependence of interdiffusion in aluminum-rich Al-Cu melts

E. Sondermann,[1,*] N. Jakse,[2] K. Binder,[1] A. Mielke,[1] D. Heuskin,[1] F. Kargl,[1] and A. Meyer[1]
[1]*Institut für Materialphysik im Weltraum, Deutsches Zentrum für Luft- und Raumfahrt (DLR), 51170 Köln, Germany*
[2]*Univ. Grenoble Alpes, CNRS, Grenoble INP, SIMaP, F-38000 Grenoble, France*

(Received 31 August 2018; revised manuscript received 25 October 2018; published 28 January 2019)

We present measurements and *ab initio* molecular dynamic simulations of interdiffusion in aluminum-rich Al-Cu melts for concentrations up to 30 at. % copper. To obtain accurate data, a combination of x-ray radiography and shear-cell technique is used, including an experiment in microgravity. Interdiffusion coefficients between 5.3 and 3.2 $\times$ 10^{-9} m^2/s at 973 K are found experimentally with a slight decrease with increasing Cu concentration. Results from *ab initio* molecular dynamic simulation at 1000 K show a decrease of interdiffusion coefficients with the same slope at slightly higher values. Using Darken's equation to discuss the relation between self-diffusion and interdiffusion, we find the cross-correlation term S to be around unity by simulation and experiment.

DOI: 10.1103/PhysRevB.99.024204

I. INTRODUCTION

Diffusion in general describes the long-range transport of particles by random motion due to their thermal energy. In liquid alloys, diffusion impacts the formation and evolution of the microstructure during solidification [1–3]. This makes diffusion coefficients in the melt an important parameter in the simulation and design of cast alloys.

Al-Cu has been established as a model system on which numerous studies were performed regarding the solidification behavior [4–7], its thermophysical properties [8–10], and the structure of the melt [11,12]. Furthermore, Al-Cu exhibits pronounced x-ray contrast, facilitating the application of *in situ* measurement techniques.

In multicomponent alloys, chemical diffusion or interdiffusion is distinguished from self-diffusion. Chemical diffusion is measured by studying the evolution of a concentration gradient. It is driven by differences in the chemical potential. Self-diffusion describes the long-range transport of a single tagged particle driven by entropy. It can be measured by studying the spreading of an isotope accumulation.

Conventionally, diffusion coefficients are measured *ex situ* by the long-capillary technique where two rods of different concentrations or different isotope contents are brought together in a thin tube. The samples are annealed at the desired temperature and the concentration or isotope distribution is analyzed after solidification. The diffusion coefficient is derived from this distribution according to Fick's law. However, the concentration or isotope distribution can be altered during melting and solidification as well as by convection due to buoyancy or free surfaces (Marangoni convection) [13–16].

In recent years new methods have been developed to overcome or reduce these effects. Self-diffusion can be accurately measured by quasielastic neutron scattering (QENS) for many liquid metals and alloys [17]. In the hydrodynamic limit, self-diffusion is related to the width of the incoherent, quasielastic signal of the dynamic structure factor. For alloys in which the incoherent part arises mainly from one element, the self-diffusion coefficient of this element can be derived. Because QENS probes the diffusion on an atomic length scale and on a picosecond time scale, its results are unperturbed by convection [18].

For the measurement of interdiffusion in liquid alloys, the combination of the long-capillary technique with x-ray radiography (XRR) greatly improved process control [19]. The diffusion process is thus studied space- and time-resolved. One time-resolved measurement by XRR corresponds to a series of ex situ measurements with different diffusion times. As the diffusion process is studied *in situ*, changes of the concentration profile during solidification do not affect the measurement. Space-resolved information allows for analyzing parts of the sample separately to reveal convection rolls [13]. Furthermore, free surfaces, which can provoke Marangoni convection in the sample, can be detected and affected measurements are excluded from analysis. As in classical long-capillary setups, the denser alloy is placed at the bottom and the convective flow is reduced by choosing a small sample-diameter [6,15].

Molecular dynamic simulation is a powerful tool to study various material properties and to extend knowledge beyond the experimentally accessible range. Results of classical molecular dynamic simulations may differ depending on the potential used [20]. These potentials can be optimized to describe melt properties using more accurate diffusion coefficients in the liquid which was shown using the example of liquid titanium [21]. On the other hand, *ab initio* molecular dynamics (AIMD) provides a very accurate tool to study consistently structural, dynamic, and electronic properties of a large variety of materials, including metallic systems [22]. This technique has proven to be particularly well suited for the study of liquid alloys and their evolution as a function of concentration, as it is able to take into account specificities of electronic structures through the density functional theory.

*elke.sondermann@dlr.de

Our first objective is to resolve the problem of the evolution of interdiffusion with concentration in liquid Al-Cu alloys since there is a controversy in the results by different research groups. The goal is achieved by using AIMD and obtaining refined measurements of interdiffusion.

To measure interdiffusion in aluminum-rich Al-Cu melts, we use an advanced setup which combines the linear shear-cell technique [23,24] and XRR. In a shear cell, rod-shaped samples of different concentrations are melted separately. When the desired temperature is reached, samples of two different concentrations are brought into contact by a shear movement of part of the sample holder. This gives the observed diffusion process a distinct starting point and avoids disturbances due to the melting process, e.g., segregation. The movement is done with a low velocity in order to minimize shear convection [25].

To exclude buoyancy-driven convection from the diffusion measurement, selected samples were additionally measured under microgravity (μg). For these experiments the same combination of x-ray radiography and shear-cell technique was implemented aboard the sounding rocket MAPHEUS.

To further verify the reliability of the measurement results, interdiffusion experiments with the diffusion couple $Al_{90}Cu_{10}$-$Al_{85}Cu_{15}$ were conducted in a classical shear cell [26]. In this approach the samples are melted separately, brought into contact by a shear movement, annealed for a defined time, and finally separated into several sections before freezing the sample. This procedure prevents changes in the concentration profile due to solidification. The sections are analyzed *ex situ* by atomic absorption spectroscopy.

The interdiffusion coefficient D_{AB} in a binary liquid alloy A-B is related to the self-diffusion coefficients D_A and D_B via the equation [27]

$$D_{AB} = S\Phi(c_A D_B + c_B D_A). \tag{1}$$

Here, c_A and c_B are the atomic concentrations of A and B, Φ is the thermodynamic factor, and S describes the influence of cross-correlations. In the microscopic description presented in Ref. [27], the factor S is due to distinct velocity correlation functions. For alloys with chemical short-range order that show a mixing tendency, S is expected to be below unity [27,28]. For $S = 1$, Eq. (1) reproduces Darken's equation [29], which is an approximation based on thermodynamic considerations.

The factor S has recently been studied by experiments and simulations in liquid Al-Ni and Ni-Zr [30–33]. These alloys show chemical short-range order and a tendency for mixing. Our second objective is to further elucidate the connection between S and the mixing tendency of liquid alloys.

II. METHODS

A. Experimental details

For the x-ray shear-cell experiment, sample materials with Cu content between 0 and 30 at. % were prepared from the pure elements (Al, 99.999% Cerac; Cu, 99.995%, Alfa Aesar) by inductive melting in a cold crucible under a purified argon atmosphere. From each alloy, rods of 1.2 mm in diameter were prepared by arc melting and suction casting into a water-cooled copper mold under a purified argon atmosphere. The capillaries containing the samples have a diameter of 1.3 mm and a total length of 15 mm. At one end of the capillary, a reservoir containing the same alloy is provided. The material in the reservoir is needed for volume compensation during melting to ensure complete filling of the capillaries.

The furnace itself is made of high-purity graphite (Mersen 2120 PT) which is high-temperature stable, is x-ray transparent, and shows no reaction with the sample material. It is heated by a resistance heater made of molybdenum wire and thermally insulated by graphite foam. The whole setup is placed inside a vacuum chamber where the pressure stays below 2×10^{-3} mbar during the measurement. Details of the furnace setup are described in Ref. [34]. To avoid segregation during melting, samples are heated in a horizontal position and turned to a vertical position when the measuring temperature of 973 K is reached.

For x-ray imaging a Viscom XT9160-TED microfocus transmission x-ray source with a tungsten target is used. It is equipped with an aperture plate with a pinhole of 0.8 mm in diameter to reduce stray radiation and is operated at 100 kV and 15 W. The x-ray detector is a Shad-o-Box 2048 by Rad-Icon with a 14-bit dynamic range and 48-μm pixel size. The positions of the x-ray source, the sample, and the detector result in an effective pixel resolution of about 25 μm. The x-ray images are continuously recorded using an exposure time of 2 s.

The gray values are extracted from the x-ray images and averaged over the width of the sample using the program ImageJ. The gray values are then converted to Cu concentrations as described in Ref. [19] using the ends of the capillary, where the initial concentration remains unaffected, as references. Additionally, the left, center, and right parts of each capillary are analyzed separately in order to detect possible convection rolls and to estimate the uncertainty of each measurement [13].

For every point in time t the obtained concentration profile c is fitted using the solution of Fick's second law for two semi-infinite rods with initial concentrations c_1 and c_2 [35]:

$$c = \frac{c_1 + c_2}{2} + \frac{c_2 - c_1}{2}\mathrm{erf}\left(\frac{x - x_0}{\sqrt{4D_{AB}t}}\right). \tag{2}$$

Here, x_0 denotes the center of the diffusion profile and erf denotes the error function. The term $\sqrt{4D_{AB}t}$ is also called the diffusion length L with D_{AB} being the diffusion coefficient. Figure 1 shows the concentration profiles of one diffusion couple at different times as an example for measurements carried out on the ground [panel (a)] and aboard the sounding rocket MAPHEUS [panel (b)]. Due to a necessary gap in the outer part of the crucible, data points in the middle of the concentration profile cannot be displayed. At the earlier point in time, the concentration profile resembles a step function. At the later point in time it has become wider as diffusion progressed. The concentration profiles are well described by the fit function, Eq. (2), shown as a red (gray) line. The squared diffusion length $L^2 = 4D_{AB}t$ gained from this fit is plotted against time. It shows a linear dependence on time as can be seen in Fig. 1. The Data of the first 20 s are excluded from analysis because of possible perturbations from the shear movement. The diffusion coefficient is then derived from a linear fit by dividing its slope by 4. Additionally, the

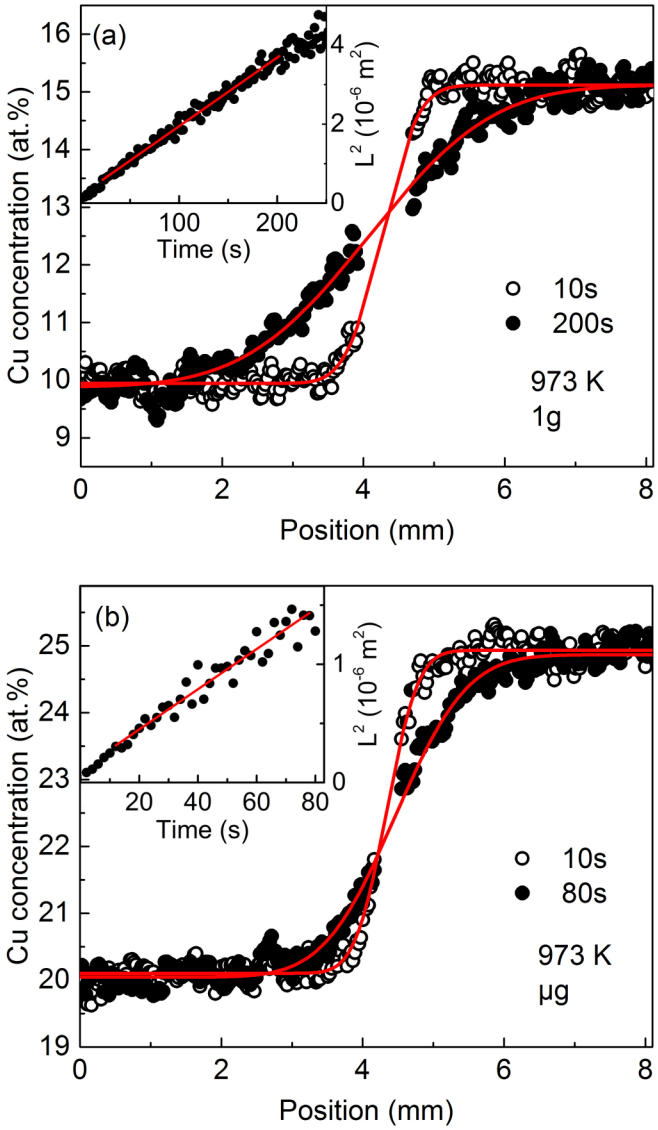

FIG. 1. Concentration profiles at two different times as obtained (a) from laboratory experiment and (b) aboard the sounding rocket MAPHEUS-5. Fits with Eq. (2) are shown as red (gray) lines. The gap in the middle of the concentration profile is due to a necessary gap in the outer part of the shear cell. The insets show the squared diffusion length L^2 derived from the concentration profiles as a function of time and a linear fit to the data.

left, center, and right parts of each capillary are analyzed separately. In cases where the diffusion coefficients from these parts differed by more then 15%, the measurement is discarded. In these cases we assume that perturbations would have affected the measurement.

To exclude disturbances of interdiffusion measurements by buoyancy, three diffusion couples ($Al_{90}Cu_{10}$-$Al_{85}Cu_{15}$, $Al_{85}Cu_{15}$-$Al_{80}Cu_{20}$, and $Al_{80}Cu_{20}$-$Al_{75}Cu_{25}$) were processed aboard the sounding rocket MAPHEUS-5. It provides a microgravity level better than 10^{-4} g. To ensure comparable conditions on the ground and in microgravity, the same shear-cell setup in combination with x-ray radiography was used. Owing to the necessary compact design of the x-ray source, it was operated at 70 kV and 10 W. The samples were already

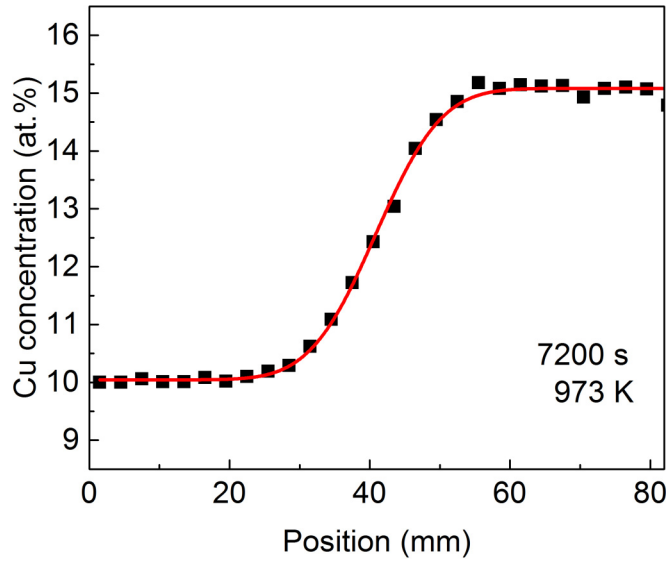

FIG. 2. Concentration profile as obtained from laboratory experiment using the *ex situ* shear cell [26]. A fit with Eq. (2) is shown as a red (gray) line.

liquid before lift-off. When the samples were homogeneous and a stable temperature was reached, the two parts of each diffusion couple were brought into contact by the shear movement and diffusion was recorded for 80 s in microgravity. Due to problems in the heater control, the temperature of the crucible was increased by 3.9 K during this time. Changes in temperature favor temperature differences which may cause convection. In two samples bubbles appeared close to the contact plane. A bubble in a concentration gradient will lead to convection due to differences in the surface tension (Marangoni convection). One of these samples cannot be analyzed, the other one yields a diffusion coefficient which is a factor 1.5 higher than the values obtained on the ground. In the third diffusion couple, only a small bubble far away from the contact plane was present and did not change its position. Such a bubble will not affect the measurement [13]. This measurement is therefore included in the discussion. Besides the 1 g and μg XRR experiments, three diffusion couples $Al_{90}Cu_{10}$-$Al_{85}Cu_{15}$ were processed at 973 K in a graphite *ex situ* shear cell. Samples were melted separately in a horizontal position. After time for homogenization, the setup was moved into a vertical position and the samples were brought into contact. The diffusion couples had a total length of 90 mm and were processed for 7200 s. This ensures a sufficient spread of the concentration profile while leaving the concentration at the capillary ends unchanged. Therefore the assumption of two semi-infinite rods in the analysis is valid. The samples were divided into sections of 3 mm in length before cooling. Further details of the setup are given in Ref. [26].

The concentration of the solidified sections were analyzed by atomic absorption spectroscopy. This concentration profile was fitted with Eq. (2) as shown in Fig. 2 and the interdiffusion coefficient was derived from the obtained diffusion length and the known diffusion time. The results of the three measurements agree with each other. For further discussion, the average value is used.

B. Computational details

The AIMD simulations of liquid Al-Cu alloys with copper concentrations of 10, 20, and 30 at. % were taken from our preceding work [36]. An additional simulation has been performed in the present work for concentration 25 at. %. All the simulations were performed within the Vienna *ab initio* simulation package [37] with projected augmented plane-waves with a cutoff of 270 eV, using the local density approximation to describe exchange-correlation effects [38,39]. A total of 256 atoms arranged in a cubic simulation box with standard periodic boundary conditions has been considered with only the Γ point to sample the Brillouin zone. We have shown that such approximations reproduce correctly the structural and transport properties of liquid aluminum [40] as well as Al-Cu liquid alloys [36]. Additionally, we mention that for these systems the generalized gradient approximation leads to overstructuring effects and a lower self-diffusion coefficient with respect to experiments. The numbers of Al and Cu atoms were chosen to reproduce the desired composition and the volume of the box was fixed to reproduce the experimental densities [8]. The molecular dynamics simulations were carried out by integrating numerically Newton's equations of motion using Verlet's algorithm in the velocity form, with a time step of 1.5 fs within the NVT ensemble by means of a Nosé thermostat to control temperature. For all compositions, the liquid samples were first simulated at a temperature well above the one studied, namely 2500 K during 30 ps to reach thermal equilibrium, and cooled down at a rate of 3×10^{12} K/s to the desired temperature of 1000 K. The pressures calculated in the simulation cell do not exceed 0.9 GPa with a typical fluctuation of 1.2 GPa. After reaching the target temperature, the run was continued for an equilibration period of 30 ps followed by an 80-ps production time during which the self-diffusion and interdiffusion were calculated. Such a simulation time is sufficiently long for performing accurate statistics but does not exceed the time for which finite-size effects could occur due to the smallness of the simulation box.

The self-diffusion coefficients were determined from the well-known Green-Kubo time integral of the velocity autocorrelation function for each species. The interdiffusion coefficients were calculated by means of the concentration current-current correlation function, expressed in terms of the Al velocities, and integrated using the Green-Kubo formalism. This is equivalent to taking the Cu velocities however the choice of Al is made to have better statistics, since Al is the majority type of atom for all concentrations used here. It contains the long-wavelength limit of the concentration-concentration structure factor in the Bhatia-Thornton formalism. The latter was obtained by a smooth extrapolation to $q = 0$ by using a square polynomial function [41]. For a more detailed description we refer the reader to the Supplemental Material [42] and our preceding work [27,33].

III. RESULTS AND DISCUSSION

A. Concentration dependence of interdiffusion

The measured interdiffusion coefficients of Al-rich Al-Cu alloys at 973 K are compiled in Fig. 3. Measurements using the linear shear-cell technique and XRR for alloys with the same concentration agree within error bars. Only at 22.5 at. % Cu is one value clearly higher than the other one. Convection which cannot be detected by XRR, e.g., helical flow or convection rolls perpendicular to the projection plane, may be the cause [13]. The value obtained in microgravity is between the interdiffusion coefficients measured on the ground, tending towards the higher value. The interdiffusion coefficient obtained with the *ex situ* shear cell is directly below the two values measured with the shear-cell technique and XRR. Overall, the coefficients measured in different environment and with different techniques show good agreement.

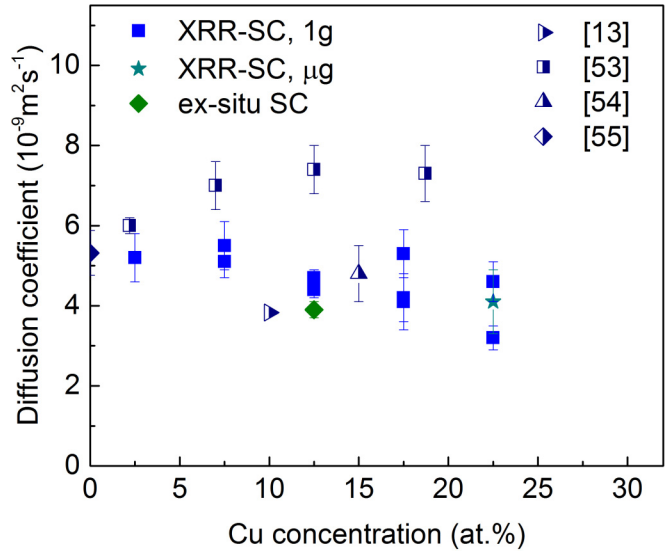

FIG. 3. Measured interdiffusion coefficients at 973 K as a function of Cu concentration. Displayed are data obtained using a combination of x-ray radiography and shear-cell technique (XRR-SC) on the ground and in microgravity as well as data using an *ex situ* shear cell. For comparison, data from literature are also shown.

For comparison, the data by Zhang *et al.* [53] which were obtained at 983 K using a combination of x-ray radiography and the long-capillary technique are also shown. These interdiffusion coefficients are higher than the ones presented here, which is due to perturbations [13].

In a setup similar to the XRR and shear-cell technique used here, Kargl *et al.* measured $D_{\mathrm{AlCu}} = 3.8 \times 10^{-9}$ m^2 s^{-1} for $Al_{90}Cu_{10}$ at 973 K [13]. Zhong *et al.* report an interdiffusion coefficient of $(4.8 \pm 0.7) \times 10^{-9}$ m^2 s^{-1} for $Al_{85}Cu_{15}$ at 993 K from a series of experiments with different diffusion times using a sliding cell [54]. Those values are compatible with the ones presented here. The same is true for measurements of impurity diffusion of Cu in Al by Ejima *et al.* [55] who found 5.3×10^{-9} m^2/s at 976 K.

Lee *et al.* [56] determined diffusion coefficients by analyzing the concentration profile ahead of a planar single phase and a planar eutectic interface in small-diameter tubes. For concentrations between 1.7 and 11.8 at. % Cu a diffusion coefficient of 2.4×10^{-9} m^2 s^{-1} was measured. Diffusion is probed in the vicinity of the eutectic temperature assuming a temperature-independent diffusion coefficient. A different way to obtain interdiffusion coefficients is to use x-ray

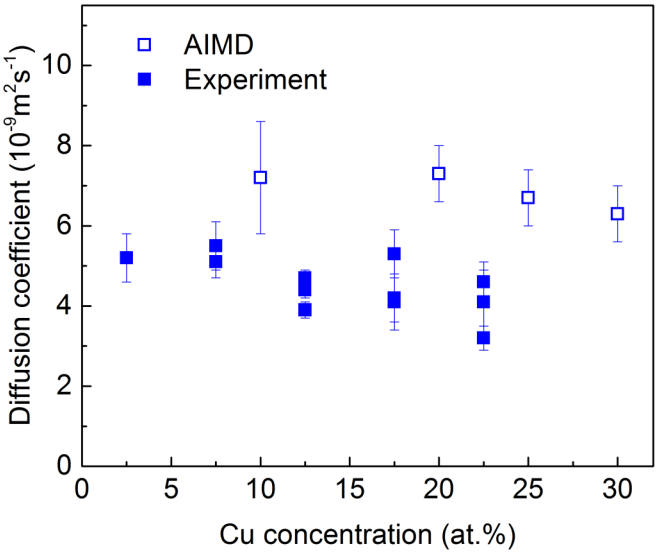

FIG. 4. Interdiffusion coefficients obtained by *ab initio* molecular dynamic simulation (AIMD) at 1000 K in comparison to experimental values at 973 K.

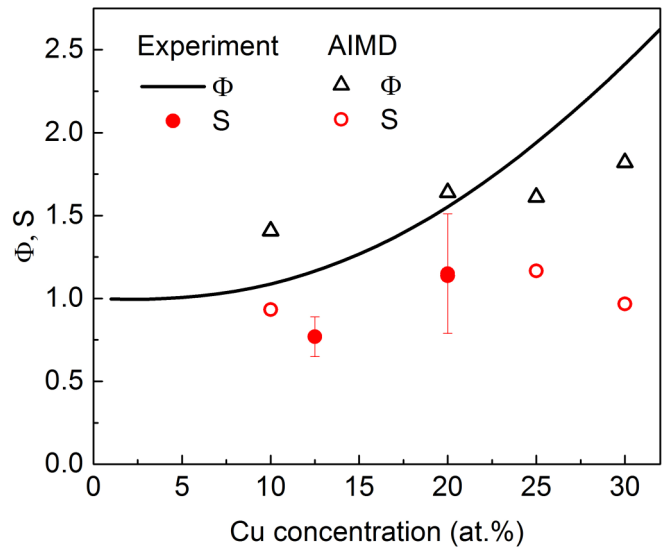

FIG. 5. Thermodynamic factor Φ and Manning factor S as a function of Cu concentration gained from experiment and *ab initio* molecular dynamic simulation. The experimental thermodynamic factor is derived from the thermodynamic description of Al-Cu by Witusiewicz *et al.* [60]. Note that at 20 at. % Cu content, the symbols for S determined by experiment and AIMD overlap.

tomography to study the coarsening of the microstructure during annealing. The results are matched with phase-field modeling. This approach was employed by Aagesen *et al.* [57] and Zhang *et al.* [58] for $Al_{93}Cu_7$ and $Al_{90.4}Cu_{9.6}$, respectively. A diffusion coefficient of 8.3×10^{-10} m^2 s^{-1} was found at 836 or 831 K, respectively.

While data from Ref. [53] suggested an increase of the diffusion coefficient with increasing Cu content, values presented here show a slight decrease. As density and dynamic viscosity are found to increase with increasing copper concentration [10,36] a slower dynamics is expected.

A reasonable agreement of experimental and simulation results can be seen in Fig. 4, keeping in mind that the simulation was done at a slightly higher temperature. The diffusion coefficients determined by AIMD indicate a slight decrease for concentrations above 20 at. % Cu with a slope similar to the one found in the experiment at 973 K. Molecular dynamic simulations presented by Trybula *et al.* [59] using the embedded atom model show a considerably larger drop of the interdiffusion coefficient by about 40% between 10 and 30 at. % Cu at 1345 K. These values should be taken with caution as they are extracted from self-diffusion coefficients, the latter being underestimated by a factor of 2 with respect to AIMD [36].

B. Influence of cross-correlations

To determine the influence of cross-correlations on interdiffusion in liquid Al-Cu, the factor S is calculated from Eq. (1). To do so, the thermodynamic factor Φ is derived from the Gibbs free energy G of liquid Al-Cu via

$$\Phi = \frac{c(1-c)}{RT}\frac{\partial^2 G}{\partial c^2}. \tag{3}$$

In this equation, c is the concentration of one component, R the gas constant, and T the absolute temperature. Φ can be derived from the Redlich-Kister polynomial coefficients for values of Gibbs free energy given by Witusiewicz *et al.* [60] or Saunders [61]. The difference between the calculated Φ is less than 6% at the discussed concentrations. In the discussion we use the thermodynamic description of Al-Cu given by Witusiewicz *et al.* [60] because it it based on a broader and more recent experimental database. The derived thermodynamic factor Φ is depicted in Fig. 5 as a black line. As can be seen, Φ rises from one to about 2.5 in the discussed concentration range. The increase of Φ calculated by AIMD is more shallow.

The self-diffusion of copper D_{Cu} at 973 K was reported for $Al_{80}Cu_{20}$ in Ref. [62] as $(2.4 \pm 0.2) \times 10^{-9}$ m^2 s^{-1} and for $Al_{87.5}Cu_{12.5}$ in Ref. [63] as $(5.3 \pm 0.07) \times 10^{-9}$ m^2 s^{-1} using QENS. These results are employed in the calculation of S. Measurements of D_{Cu} by Dahlborg *et al.* [64] using also QENS but employing a jump diffusion model to analyze the data gives higher values which decrease from 7×10^{-9} m^2 s^{-1} at 10 at. % Cu to 5.5×10^{-9} m^2 s^{-1} at 25 at. % Cu. For a discussion we refer the reader to Ref. [63].

Due to the lack of suitable isotopes and the very low incoherent scattering cross section of aluminum, there are no measurements of D_{Al} in Al-Cu. In the following calculations we assume $D_{Al} = D_{Cu}$. Using $D_{Al} \approx 1.1 \times D_{Cu}$ as suggested by AIMD simulation [36] changes the result for S by less than 2%. The value of D_{Al} has a minor effect on the calculation of S in aluminum-rich alloys because it is weighted with the low concentration of copper, as can be seen from Eq. (1).

For the calculation the average of the two interdiffusion coefficients measured by XRR at 12.5 at. % Cu was used. To estimate the interdiffusion coefficient at 20 at. % Cu, the values at 17.5 and 22.5 at. % Cu were averaged.

Figure 5 shows the cross-correlation term S which was calculated according to Eq. (1) using experimental data denoted as solid red circles. The resulting values for S at 12.5 and 20 at. % Cu are slightly below and slightly above unity, respectively. Results from AIMD simulations are depicted as open red circles in Fig. 5. Note that at 20 at. % Cu, the values for S from the experiment and the simulation overlap. AIMD simulations indicate that for concentrations between 10 and 30 at.% Cu S is close to unity without a clear composition dependence. This is in line with findings by Trybula *et al.* [65] and Wang *et al.* [66] who calculated S to equal unity in $Al_{80}Cu_{20}$.In a recent study on aluminum-rich Al-Ni, S was found to be between 0.7 and 0.8 [30]. Also molecular dynamic simulations [32] and *ab initio* molecular dynamics [33] found S to be below unity in Al-Ni melts. In liquid Ni-Zr values between 0.3 and 0.65 were obtained for concentrations between $Zr_{36}Ni_{64}$ and $Zr_{64}Ni_{36}$ [31]. Just like Al-Ni and Ni-Zr, Al-rich Al-Cu exhibits chemical short-range order in the liquid phase with a preference of unlike atoms to pair [9,36]. From these three materials, Al-Cu has the smallest negative enthalpy of mixing [60] followed by Al-Ni [67]. Ni-Zr has the largest negative enthalpy of mixing [68] in the respective concentration range. This corresponds to a decrease of S. It appears that interdiffusion is more influenced by cross-correlations the stronger the mixing tendency is.

IV. SUMMARY

Accurate interdiffusion coefficients in Al-Cu melts were measured for concentrations between 2.5 and 22.5 at.% copper at 973 K using an advanced setup which combines x-ray radiography and the linear shear-cell technique. An experiment in microgravity confirmed that buoyancy did not disturb these measurements. Independent measurements using an *ex situ* shear cell matched the results. Interdiffusion coefficients in Al-rich Al-Cu lay between 5.3 and 3.2×10^{-9} m^2/s at 973 K, showing a slight decrease with increasing Cu-concentration. Above a copper concentration of 20 at. %, AIMD and experiment indicate a decrease of the interdiffusion coefficients with comparable slope. Experiments and simulations suggest that the influence of cross-correlations on interdiffusion in Al-Cu is weaker compared to values reported for Al-Ni and Ni-Zr.

ACKNOWLEDGMENTS

N.J. acknowledges the CINES and IDRIS under Project No. INP2227/72914 as well as PHYNUM CIMENT for computational resources. His work was performed within the framework of the Centre of Excellence of Multifunctional Architectured Materials (CEMAM) Grant No. nANR-10-LABX-44-01 funded by the Investments for the Future Program.

[1] G. Kasperovich, A. Meyer, and L. Ratke, Int. Foundry Res. **62**, 8 (2010).
[2] L. Zhang, Y. Du, I. Steinbach, Q. Chen, and B. Huang, Acta Mater. **58**, 3664 (2010).
[3] H. Nguyen-Thi, G. Reinhart, G. Salloum-Abou-Jaoude, D. Browne, A. Murphy, Y. Houltz, J. Li, D. Voss, A. Verga, R. Mathiesen, and G. Zimmermann, Microgravity Sci. Technol. **26**, 37 (2014).
[4] R. H. Mathiesen, L. Arnberg, K. Ramsøskar, T. Weitkamp, C. Rau, and A. Snigirev, Metall. Mater. Trans. B **33**, 613 (2002).
[5] M. Gündüz and E. Çadirli, Mat. Sci. Eng., A **327**, 167 (2002).
[6] R. Trivedi, H. Miyahara, P. Mazumder, E. Simsek, and S. Tewari, J. Cryst. Growth **222**, 365 (2001).
[7] H. Dong and P. Lee, Acta Mater. **53**, 659 (2005).
[8] J. Brillo, I. Egry, and J. Westphal, Int. J. Mater. Res. **99**, 162 (2008).
[9] Y. Odusote, J. Non-Cryst. Solids **402**, 96 (2014).
[10] Y. Plevachuk, V. Sklyarchuk, A. Yakymovych, S. Eckert, B. Willers, and K. Eigenfeld, Metall. Mater. Trans. A **39**, 3040 (2008).
[11] N. Jakse and A. Pasturel, AIP Adv. **7**, 105212 (2017).
[12] L. H. Xiong, X. D. Wang, Q. P. Cao, D. X. Zhang, H. L. Xie, T. Q. Xiao, and J. Z. Jiang, J. Phys.: Condse. Matter **29**, 035101 (2017).
[13] F. Kargl, E. Sondermann, H. Weis, and A. Meyer, High Temp.-High Pressure **42**, 3 (2013).
[14] R. Roşu-Pflumm, W. Wendl, G. Müller-Vogt, S. Suzuki, K.-H. Kraatz, and G. Frohberg, Int. J. Heat Mass Transfer **52**, 6042 (2009).
[15] H. Müller and G. Müller-Vogt, Cryst. Res. Technol. **38**, 707 (2003).
[16] J. I. D. Alexander, J.-F. Ramus, and F. Rosenberger, Microgravity Sci. Technol. **9**, 158 (1996).
[17] A. Meyer, EPJ Web Conf. **83**, 01002 (2015).
[18] A. Meyer, Phys. Rev. B **81**, 012102 (2010).
[19] A. Griesche, B. Zhang, E. Solórzano, and F. Garcia-Moreno, Rev. Sci. Instrum. **81**, 056104 (2010).
[20] J. Dziedzic, S. Winczewski, and J. Rybicki, Comp. Mater. Sci. **114**, 219 (2016).
[21] J. Horbach, R. E. Rozas, T. Unruh, and A. Meyer, Phys. Rev. B **80**, 212203 (2009).
[22] J. Hafner, J. Comput. Chem. **29**, 2044 (2008).
[23] C. Neumann, E. Sondermann, F. Kargl, and A. Meyer, J. Phys.: Conf. Ser. **327**, 012052 (2011).
[24] E. Sondermann, C. Neumann, F. Kargl, and A. Meyer, High Temp.-High Pressure **42**, 23 (2013).
[25] S. Suzuki, K.-H. Kraatz, and G. Frohberg, Microgravity Sci. Technol. **18**, 155 (2006).
[26] D. Heuskin, F. Kargl, A. Griesche, C. Stenzel, D. Mitschke, D. Bräuer, and A. Meyer, J. Phys.: Conf. Ser. **327**, 012053 (2011).
[27] J. Horbach, S. K. Das, A. Griesche, M.-P. Macht, G. Frohberg, and A. Meyer, Phys. Rev. B **75**, 174304 (2007).
[28] I. V. Belova, T. Ahmed, U. Sarder, A. V. Evteev, E. V. Levchenko, and G. E. Murch, Philos. Mag. **97**, 230 (2017).
[29] L. S. Darken, Trans. AIME **175**, 184 (1948).
[30] E. Sondermann, F. Kargl, and A. Meyer, Phys. Rev. B **93**, 184201 (2016).
[31] F. Yang, P. Heintzmann, F. Kargl, K. Binder, B. Nowak, B. Schillinger, T. Voigtmann, and A. Meyer, Phys. Rev. B **98**, 064202 (2018).
[32] P. Kuhn, J. Horbach, F. Kargl, A. Meyer, and T. Voigtmann, Phys. Rev. B **90**, 024309 (2014).

[33] N. Jakse and A. Pasturel, J. Chem. Phys. **143**, 084504 (2015).
[34] K. Binder, F. Kargl, and C. Stenzel (unpublished).
[35] J. Crank, *The Mathematics of Diffusion*, 2nd ed. (Oxford University, Oxford, England, 1999).
[36] N. Jakse and A. Pasturel, Phys. Rev. B **94**, 224201 (2016).
[37] G. Kresse and J. Furthmüller, Comput. Mater. Sci. **6**, 15 (1996).
[38] D. M. Ceperley and B. J. Alder, Phys. Rev. Lett. **45**, 566 (1980).
[39] J. P. Perdew and A. Zunger, Phys. Rev. B **23**, 5048 (1981).
[40] N. Jakse and A. Pasturel, Sci. Rep. **3**, 3135 (2013).
[41] Y. Waseda, *The Structure of Non-Crystalline Materials: Liquids and Amorphous Solids* (McGraw–Hill, New York, 1980).
[42] See Supplemental Material at http://link.aps.org/supplemental/10.1103/PhysRevB.99.024204 for more specifics on the AIMD simulations, which include Refs. [43–52].
[43] G. Kresse and D. Joubert, Phys. Rev. B **59**, 1758 (1999).
[44] N. Jakse and A. Pasturel, Phys. Rev. Lett. **91**, 195501 (2003).
[45] N. Jakse and A. Pasturel, Sci. Rep. **6**, 20689 (2016).
[46] N. Jakse and A. Pasturel, Phys. Rev. B **95**, 144210 (2017).
[47] A. Pasturel and N. Jakse, npj Comput. Mater. **3**, 33 (2017).
[48] A. Pasturel and N. Jakse, Appl. Phys. Lett. **110**, 121902 (2017).
[49] N. Jakse and A. Pasturel, J. Chem. Phys. **144**, 244502 (2016).
[50] M. Schick, J. Brillo, I. Egry, and B. Hallstedt, J. Mater. Sci. **47**, 8145 (2012).
[51] N. Y. Konstantinova, P. S. Popel', and D. A. Yagodin, High Temp. **47**, 336 (2009).
[52] J.-P. Hansen and I. R. McDonald, *Theory of Simple Liquids*, 2nd ed. (Academic, London, 1986).
[53] B. Zhang, A. Griesche, and A. Meyer, Phys. Rev. Lett. **104**, 035902 (2010).
[54] L. Zhong, J. Hu, Y. Geng, C. Zhu, and B. Zhang, Rev. Sci. Instrum. **88**, 093905 (2017).
[55] T. Ejima, T. Yamamura, N. Uchida, Y. Matsuzaki, and M. Nikaido, J. Jpn. Inst. Met. **44**, 316 (1980).
[56] J. Lee, S. Liu, H. Miyahara, and R. Trivedi, Metall. Mater. Trans. B **35**, 909 (2004).
[57] L. Aagesen, J. Fife, E. Lauridsen, and P. Voorhees, Scr. Mater. **64**, 394 (2011).
[58] J. Zhang, S. O. Poulsen, J. W. Gibbs, P. W. Voorhees, and H. F. Poulsen, Acta Mater. **129**, 229 (2017).
[59] M. E. Trybula, P. W. Szafrański, and P. A. Korzhavyi, J. Mater. Sci. **53**, 8285 (2018).
[60] V. T. Witusiewicz, U. Hecht, S. G. Fries, and S. Rex, J. Alloys Compd. **385**, 133 (2004).
[61] N. Saunders, in *COST507-Thermophysical Database for Light Metal Alloys*, edited by Ansara, A. T. Dinsdale, and M. H. Rand (European Communities, Luxembourg, 1998), Vol. 2, p. 28.
[62] J. Brillo, S. M. Chathoth, M. M. Koza, and A. Meyer, Appl. Phys. Lett. **93**, 121905 (2008).
[63] F. Kargl, H. Weis, and A. Meyer (unpublished).
[64] U. Dahlborg, M. Besser, M. Kramer, J. Morris, and M. Calvo-Dahlborg, Physica B (Amsterdam, Neth.) **412**, 50 (2013).
[65] M. Trybula, T. Gancarz, and W. Gasior, Fluid Phase Equilib. **421**, 39 (2016).
[66] W. Wang, J. Han, H. Fang, J. Wang, Y. Liang, S. Shang, Y. Wang, X. Liu, L. Kecskes, S. Mathaudhu, X. Hui, and Z. Liu, Acta Mater. **97**, 75 (2015).
[67] I. Ansara, N. Dupin, H. L. Lukas, and B. Sundman, J. Alloys Compd. **247**, 20 (1997).
[68] G. Ghosh, J. Mater. Res. **9**, 598 (1994).